1. Supplementary Figures and Legends

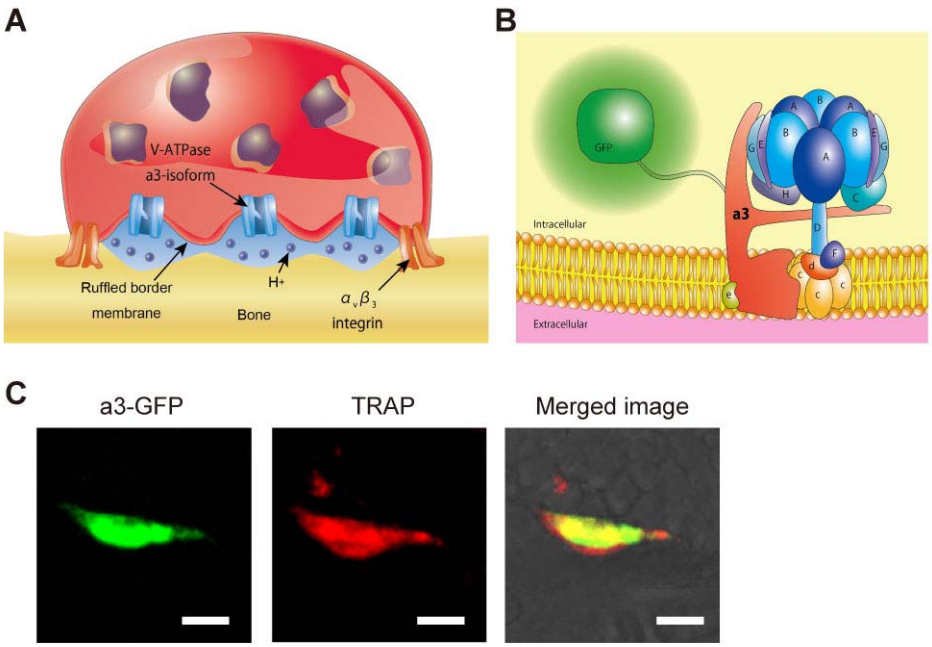

Supplementary Figure 1. V-type H^+-ATPase a3 subunit-GFP knock-in mice. **A,** Diagrammatic representation of fully differentiated mature osteoclasts. They adhere to bone surfaces sealing zones inside which a ruffled membrane is formed. Vacuolar (V)-type H^+-ATPases are expressed along the ruffled border membrane. **B,** Schematic illustration of V-type H^+-ATPase. We generated a3-GFP knock-in mice, where GFP is fused with the a3 subunit and expressed under the control of original promoter of the a3 subunit. **C**, Histological analysis of femoral bone tissues of a3-GFP knock-in mice. Fluorescent images showing a3-GFP (*green - left panel*), TRAP (tartrate-resistant acid phosphatase) for identifying mature osteoclasts (*red - middle panel*), and an overlay of the two fluorescent images with a transmission image showing the bone surface (*right panel*). Scale bars represent 10 μm.

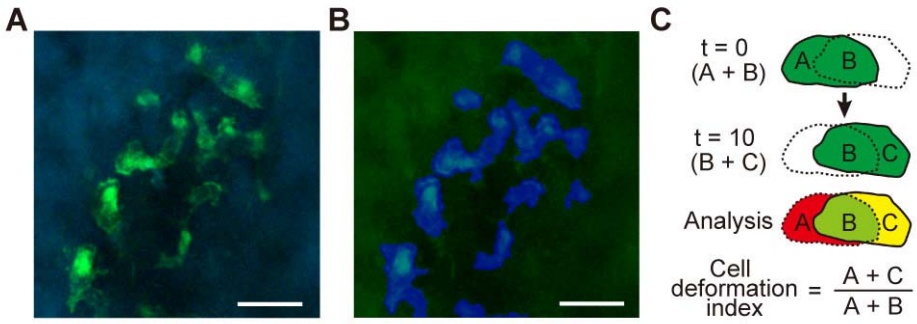

Supplementary Figure 2. Image data analysis for tracking morphological changes of mature osteoclasts. A, A representative image of intravital multiphoton microscopy of mouse bone tissues using homozygous a3-GFP knock-in mice (same as Figure 1**A**). Scale bar represents 40 μm. **B,** Blue areas represent cell shapes that are recognized automatically by the image analysis software CL-Quant 2.30. Scale bar represents 40 μm. **C,** The cell deformation index (CDI) is defined as the ratio of the cell areas changed during 10 minutes (A + C) divided by those of the previous time frame (A + B) (Supplementary Video 2). In detail, CDI was calculated as follows:

(1) Acquire frames every ten minutes from time-lapse images.

(2) Identify cells automatically on each selected frame. This software also identifies and labels the area of each cell through the different time frames.

(3) Calculate cell deformation index of each cell in each time frame. The cell deformation index is defined as the ratio of the cell areas changed during 10 minutes (A + C) divided by those of a previous time frame (A + B).

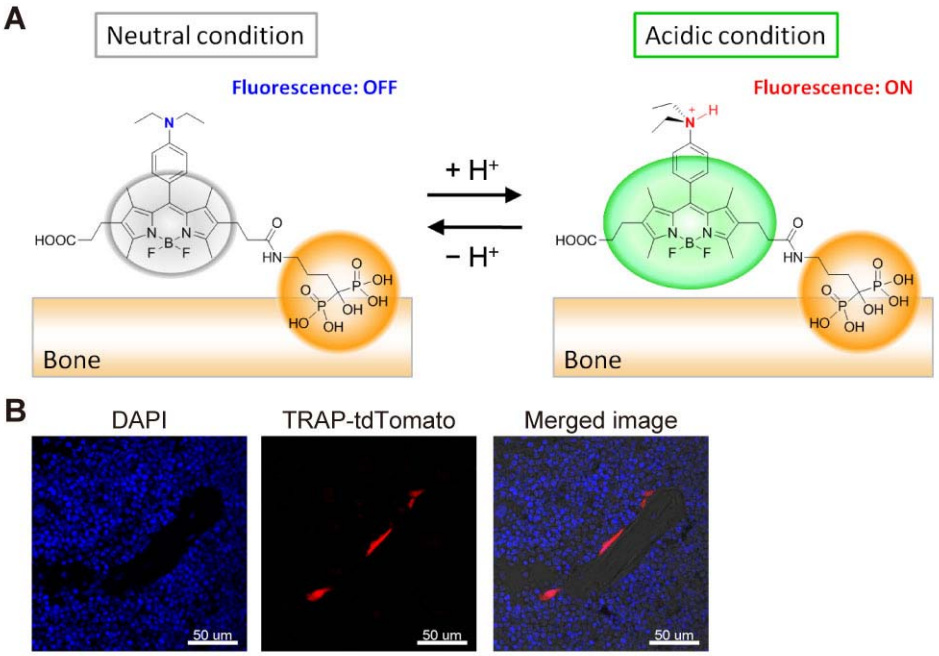

Supplementary Figure 3. A chemical fluorescent probe for detecting local bone resorption (H^+ secretion) and a TRAP promoter-driven tdTomato transgenic mice for detecting mature osteoclasts A, Schematic representation of the chemistry of a bone-attaching H^+ sensing fluorescent probe, BAp-E. **B,** Histological analysis of femoral bone tissues of TRAP-tdTomato transgenic mice. TRAP-tdTomato positive cells can be seen along the bone surface (*red*). Nuclei were stained for DAPI (*blue*). Scale bars represent 50 μm.

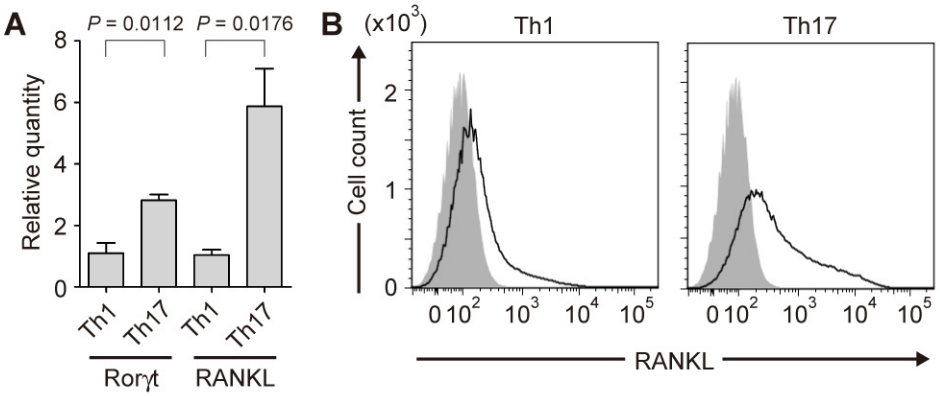

Supplementary Figure 4. Analysis of gene expression and RANKL expression in differentiated Th1 and Th17 cells *in vitro*. A, mRNA for Rorγt and RANKL were detected by quantitative RT–PCR (normalized by expression of GAPDH). RT, reverse transcription. **B,** Cell surface expression of RANKL in Th1 (*left panel*) and Th17 (*right panel*) analyzed by flow cytometry. We confirmed that RANKL was preferentially expressed on the cell surface of Th17, compared as Th1.

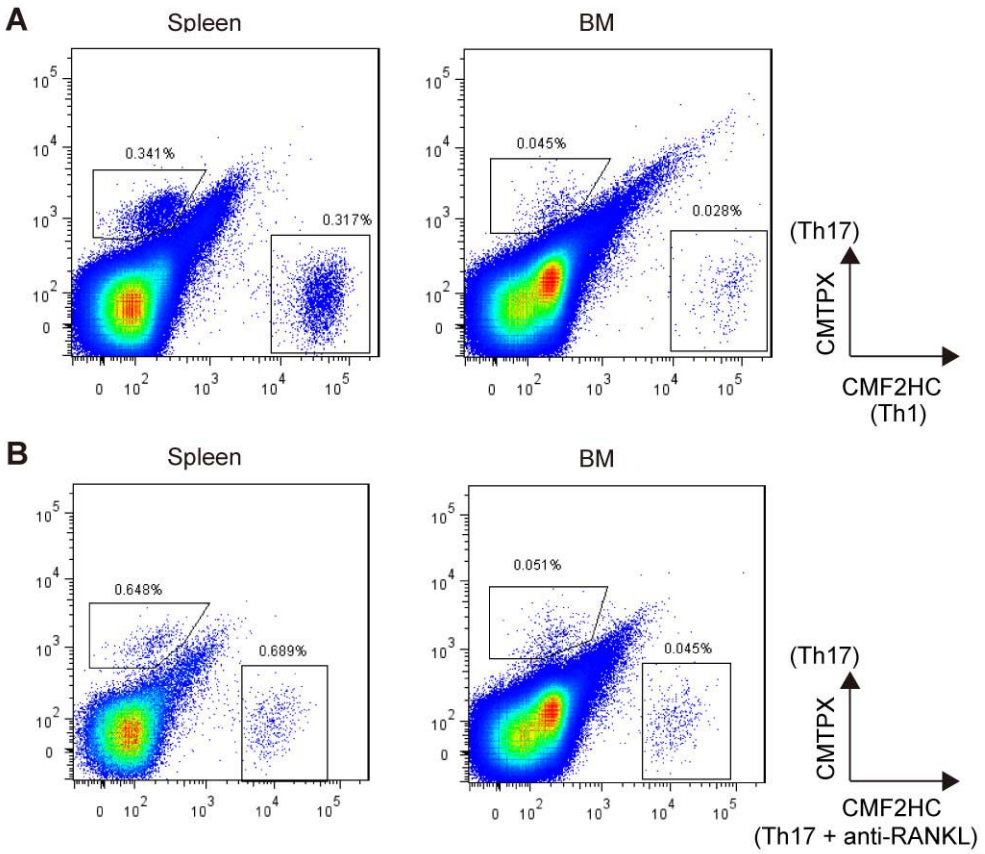

Supplementary Figure 5. FACS analysis of Th1 and Th17 cells in spleen and bone marrow of a3-GFP mice after adoptive transfer. A, Th1 (labeled with CMF2HC) and Th17 cells (labeled with CMTPX) were transferred into a3-GFP mice. After acquisition of multiphoton images, splenocytes (*left panel*) and bone marrow cells (*right panel*) were collected from the mice and analyzed using a FACS Canto II. **B,** anti-RANKL antibody treated-Th17 cells (labeled with CMF2HC) and non-treated Th17 cells (labeled with CMTPX) were transferred into a3-GFP mice. After imaging, splenocytes (*left panel*) and bone marrow cells (*right panel*) were collected from the mice and analyzed using a FACS Canto II.

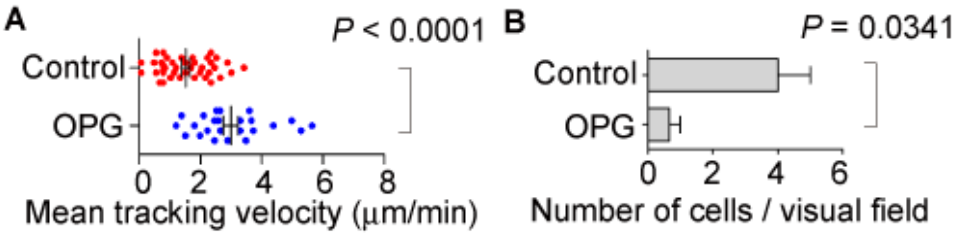

Supplementary Figure 6. Pretreatment of Th17 with osteoprotegerin (OPG) abrogates association with osteoclasts. A, Summary of mean tracking velocities of Th17 cells treated with or without osteoprotegerin (OPG). Data points (n = 24 for non-treated Th17 cells (Non) and n = 40 for Th17 cells treated with OPG) represent individual cells compiled from three independent experiments. **B,** The number of Th17 cells treated with or without OPG attached to mature osteoclasts for more than 5 minutes (n = 3, from three independent experiments). Although both OPG and anti-RANKL neutralizing antibody (Fig. 5E and F) significantly suppress the interaction between Th17 and osteoclasts, OPG seemed to be less effective. Although we do not know the exact reasons, we suppose that OPG might be dissociated from RANKL on the surface of Th17 during transfer into systemic circulation of mice. Unlike the anti-RANKL neutralizing antibody that makes a firm association as an antigen-antibody complex reaction (Kd of ~ 3 pM in the case of denosumab, an anti-human RANKL neutralizing antibody) (38), OPG is a decoy receptor for RANKL and should undergo certain association/dissociation transition (Kd ~ 10 nM) (39) . For the reason, OPG is less potent for inhibiting Th17-OC interaction in our experimental condition.

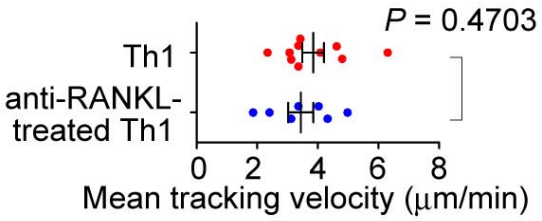

Supplementary Figure 7. Summary of mean tracking velocities of Th1 cells treated with or without anti-RANKL neutralizing antibody. Anti-RANKL antibody does not affect the mobility of bone-localized Th1 cells**.** Data points (n = 10 for non-treated Th1 cells and n = 7 for Th1 cells treated with anti-RANKL antibody) represent individual cells compiled from three independent experiments.

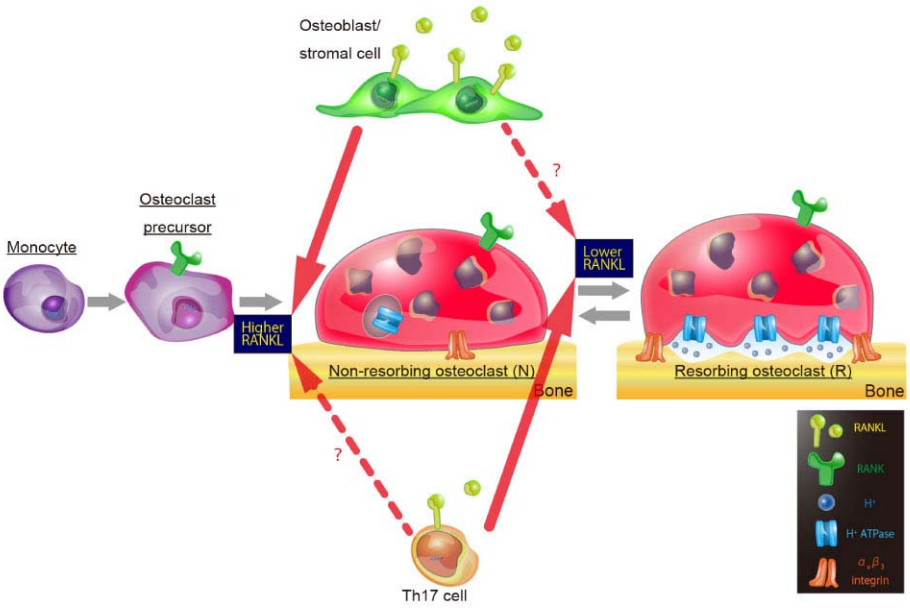

Supplementary Figure 8. Schematic illustration of RANKL-mediated control of differentiation and function of osteoclasts *in vivo*. Mature osteoclasts are formed from monocytoid osteoclast precursors by RANKL supplied from osteoblasts and/or bone marrow stromal cells. In terms of their bone-resorbing activity, there are two types of mature osteoclasts, i.e., static ‘resorbing (R)’ and moving ‘non-resorbing (N)’, and RANKL also regulates the transition between these states. The amount of RANKL required for this N to R conversion of mature osteoclasts is less than that required for induction of differentiation, and RANKL expressed on Th17, which is insufficient for induction of osteoclast differentiation, can still efficiently induce N to R transition of osteoclasts *in vivo*.

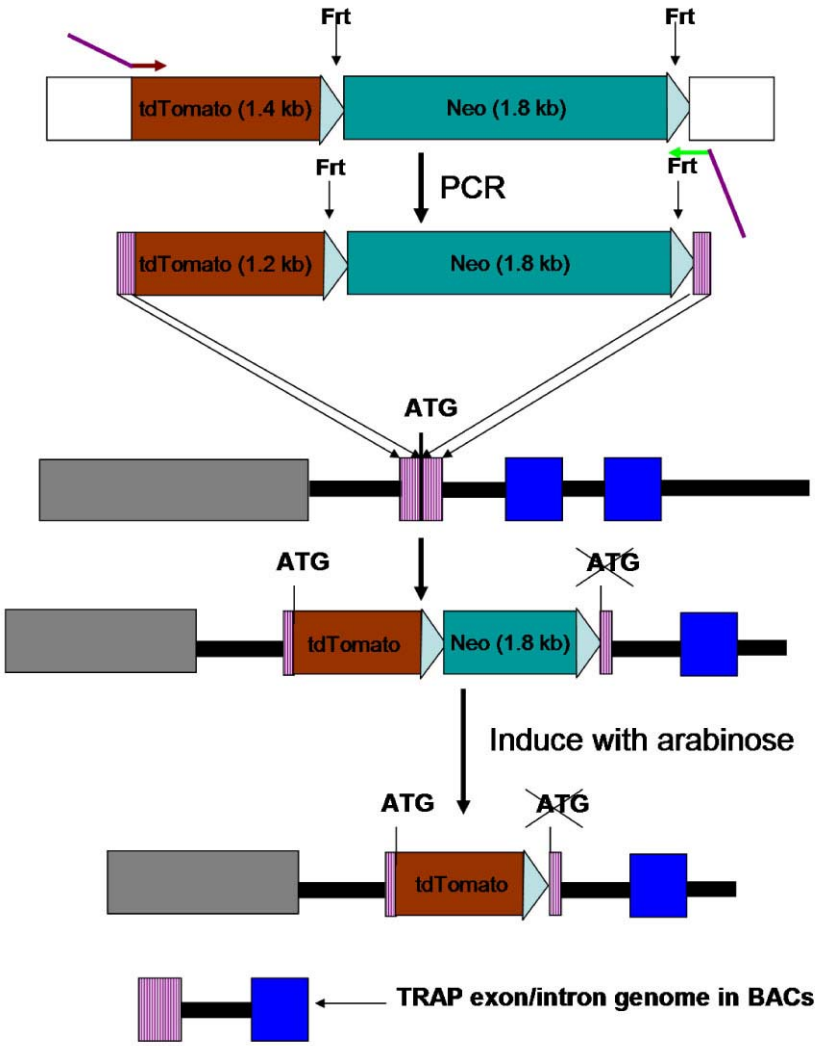

Supplementary Figure 9. The generation of the TRAP promoter-tdTomato transgenic mice. A tdTomato cDNA was inserted into the pL451 vector containing an Frt-PGK-promoter-Neo-Frt cassette. Forward primers and reverse primers were used to amplify a fragment containing tdTomato cDNA as well as the homologous sequences flanking the mouse TRAP ATG start codon site. The sequences of these primers were matched to the sequences before and after the start codon ATG of TRAP. The resulting PCR product was transfected into SW105 bacteria carrying RP24-75C9 according to standard procedures. The kanamycin-resistant clones were further screened using a PCR screening

protocol. The Frt-PGK-promoter-Neo-Frt cassette in positive BAC clones was deleted by inducing FLP recombinase, followed by confirmation using BAC DNA sequencing. The purified RP24-75C9-TRAP-tdTomato DNA was microinjected into the pronucleus of B6 fertilized eggs and founders screened by PCR screening method with the primers which just located outside regions of tdTomato. In addition, the bone samples were taken from offspring of founders and checked their expression of tdTomato by histochemistry.

2. Supplementary Video Legends

Supplementary Video 1. Intravital multiphoton imaging of mouse skull bone tissues in a3-GFP knock-in mice. Sequential images in the same visual field were acquired in control conditions. A number of large multinuclear osteoclasts are seen on the bone surface. The a3-GFP positive cells, the microvasculature of BM tissues (visualized by intravenous injection of 70 kD dextran-conjugated Texas red), and bone matrices (visualized using second harmonic imaging) are shown as green, red, and blue, respectively. Scale bar, 40 μm. Playback speed is 300x.

Supplementary Video 2. The method of an image data analysis. The movie represents how we track the morphological changes of mature osteoclasts and calculate the cell deformation index (CDI) using a specific set of image frames.

Supplementary Video 3. Intravital multiphoton imaging of mouse skull bone tissues in a3-GFP knock-in mice. Sequential images in the same visual field were acquired 2 days after intraperitoneal injection of GST-RANKL (1 mg/kg). The number of mature osteoclasts was increased. The a3-GFP positive cells, the microvasculature of BM tissues (visualized by intravenous injection of 70 kD dextran-conjugated Texas red), and bone matrices (visualized using second harmonic imaging) are shown as green, red, and blue, respectively. Scale bar, 40 μm. Playback speed is 300x.

Supplementary Video 4. Intravital multiphoton imaging of mouse skull bone tissues in a3-GFP knock-in mice. Sequential images in the same visual field were acquired after treatment with GST-RANKL and risedronate. The

number of mature osteoclasts was decreased. The a3-GFP positive cells, the microvasculature of BM tissues (visualized by intravenous injection of 70 kD dextran-conjugated Texas red) and bone matrices (visualized using second harmonic imaging) were seen as green, red, and blue, respectively. Scale bar, 40 μm. Playback speed is 300x.

Supplementary Video 5. Intravital multiphoton imaging of mouse skull bone tissues in TRAP-tdTomato transgenic mice. Sequential images in the same visual field were acquired after treatment of BAp-E. Large $TRAP^+$ cells (red) are seen on the bone surface, and the two different subsets in terms of their motility can be seen (moving and stationary), similar to what was seen in a3-GFP knock-in mice. Green fluorescent signals from H^+ probes overlapped with static, but not moving, osteoclasts. Bone matrices (visualized using second harmonic imaging) are shown as blue. Scale bar, 40 μm. Playback speed is 600x.

Supplementary Video 6. Intravital multiphoton imaging of mouse skull bone tissues in a3-GFP knock-in mice. Sequential images in the same visual field were acquired for 40 minutes before GST-RANKL injection (in control condition). Thereafter, GST-RANKL was rapidly injected intravenously. Moving mature osteoclasts rapidly convert into static cells after RANKL injection. The a3-GFP positive cells, the microvasculature of BM tissues (visualized by intravenous injection of 70 kD dextran-conjugated Texas red), and bone matrices (visualized using second harmonic imaging) are shown as green, red, and blue, respectively. Scale bar, 40 μm. Playback speed is 600x.

Supplementary Video 7. Intravital multiphoton imaging of mouse skull

bone tissues in a3-GFP knock-in mice. Sequential images in the same visual field were acquired after *in vitro* differentiated Th1 and Th17 cells were transferred intravenously. The a3-GFP–positive cells, Th1, and Th17 cells are shown as green, blue and red, respectively. Scale bar, 50 μm. Playback speed is 300x.

Supplementary Video 8. Intravital multiphoton imaging of mouse skull bone tissues in a3-GFP knock-in mice. Sequential images in the same visual field were acquired after *in vitro* differentiated Th17 cells pre-incubated with or without anti-RANKL neutralizing monoclonal antibody were transferred intravenously. The a3-GFP-positive cells are shown as green. Th17 cells treated with or without anti-RANKL antibody appear blue or red, respectively. Scale bar, 50 μm. Playback speed is 300x.

Supplementary Video 9. Intravital multiphoton imaging of mouse skull bone tissues in a3-GFP knock-in mice. Sequential images in the same visual field were acquired after *in vitro* differentiated Th17 cells were transferred intravenously. The a3-GFP-positive cells are shown as green. Th17 cells appear red. Scale bar, 20 μm. Playback speed is 300x.

3. Supplementary References

38. Elliott R, Kostenuik PJ, Chen C, et al. Denosumab is a selective inhibitor of human receptor activator of NF-KB ligand (RANKL) that blocks osteoclast formation and function. *Osteoporos Int.* 2007;18:S54

39. Schneeweis LA, Willard D, Milla ME. Functional dissection of osteoprotegerin and its interaction with receptor activator of NF-kappaB ligand. *J Biol Chem.* 2005;280(50):41155-41164.